Prediction of Periodic Loadings on Single Rotation Propfan with Off-Axis Inflow

Shih H. Chen*
Rockwell International Corporation, Canoga Park, California 91303

A three-dimensional Green's function potential paneling method is used to predict the propfan unsteady load in a yawed flow condition when the axis of blade rotation is inclined to the freestream. Unsteady response is predicted in a frequency domain with proper predetermined interblade phase angle. The method is shown to be accurate and efficient in computation comparing to a time-domain calculation. Single-rotation propfan blade SR2 is used to demonstrate the capability. The effects of shaft angle of attack, advance ratio, number of blades, and Mach number on the response due to the off-axis inflow are studied. The results indicate that the shaft angle of attack has a major effect on the unsteady blade loading.

Nomenclature

A = area
$\bar{B}_{ij}$ = steady source influence coefficient
$\tilde{b}_{ij}$ = unsteady source influence coefficient
$\bar{C}_{ij}$ = steady blade doublet influence coefficient
C_Q = torque coefficient
C_P = power coefficient
C_p = pressure coefficient
C_T = thrust coefficient
$\tilde{c}_{ij}$ = unsteady blade doublet influence coefficient
D = blade diameter
l = blade index
NB = number of blades
NT = current time step
n = surface unit normal
P = power
p' = perturbation pressure
Q = torque
R = distance between two points
r_{tip} = blade tip radius
S = boundary surface
T = period of excitation or thrust
t = time
U_x = axial freestream velocity
U_y = side wind velocity
U_∞ = freestream velocity
v_n = blade surface normal velocity
W_{iw} = steady wake doublet influence coefficient
$\tilde{w}_{iw}$ = unsteady wake doublet influence coefficient
Δt = time step
$\Delta\bar{\phi}_{\text{te}}$ = steady potential jump at blade trailing edge
$\Delta\tilde{\phi}_{\text{te}}$ = unsteady potential jump across blade surface at trailing edge
$\Delta\bar{\phi}_w$ = steady potential jump across the wake
$\Delta\tilde{\phi}_w$ = unsteady potential jump across the wake at trailing edge
θ = azimuth angle
ρ = density
σ = interblade phase angle
φ = interwake element phase angle
ϕ = velocity potential
$\tilde{\phi}_{\text{te}_l}$ = unsteady potential at blade trailing edge (lower)
$\bar{\phi}_{\text{te}_u}$ = steady potential at blade trailing edge (upper)
$\tilde{\phi}_{w_l}$ = unsteady potential on lower surface of wake at trailing edge
$\tilde{\phi}_{w_u}$ = unsteady potential on upper surface of wake at trailing edge
Ω = blade rotational speed
ω = blade rotational velocity

Subscripts

l = lower surface
o = reference blade
st = steady part
u = upper surface
un = unsteady part
w = wake
x,y,z = x,y,z component

Superscripts

$\bar{}$ = mean value
$\tilde{}$ = unsteady value

Introduction

THE new generation of turboprop (propfan) has drawn much attention because of its potential of attaining very high efficiency at high subsonic Mach numbers. As the propfan is designed to be thin, unshrouded, and flown at high speeds, the noise and aeroelastic characteristics are of great concern to engineers. One of the major propfan blade design considerations is noise level and forced response resulting from angled flow into the rotor. At level flight condition, the flow for a single rotation propfan is nearly parallel to the axis of blade rotation. The loading on the blades can be assumed steady and identical on all blades since each blade is subjected to the same angle of attack and relative velocity. When the aircraft is ascending, descending, turning, or encountering a transverse gust, the flow on the blades and their wakes are skewed due to the resultant inflow not being parallel to the rotating axis. The skewness of the flowfield depends on the angle between the inflow and the axis of rotation. This causes the blade angle of attack to change with respect to the blade circumferential position. Thus, each blade experiences a one cycle per revolution unsteady excitation. Researchers[1-9] found that the unsteadiness not only affects the noise amplitude,

Presented as Paper 89-2694 at the AIAA/ASME/SAE/ASEE 25th Joint Propulsion Conference, Monterey, CA, July 10-12, 1989; received Aug. 24, 1989; revision received June 18, 1990; accepted for publication June 20, 1990.

*Member of Technical Staff, Rocketdyne Division, MS IA34, 6633 Canoga Ave.

directivity, and aeroelastic behavior, but also the stability and control in these operating conditions. Also, the high vibratory stress caused by the resulting unsteady loading can lead to high cycle fatigue failures. The accurate prediction of the unsteady loads in these operating conditions is thus very important.

Recent studies have successfully predicted the performance for single-rotation propfan[10-14] and for counter-rotation propfan.[15-17] These analyses are mostly based on the assumption of level flight condition where the inflow is parallel to the axis of rotation. Padula and Block[5] predicted the propfan noise in angled inflow by using classical quasisteady aerodynamic prediction. Nallasamy et al.[9] solved Euler equations to predict the propfan pressure and noise at takeoff and landing Mach numbers, but no shaft angle of attack effect was included. Kaza et al.[4] and Williams and Hwang[18] also developed a three-dimensional lifting surface theory for the prediction of steady and unsteady aerodynamic and aeroelastic response of the propfan and have shown results to be accurate in comparison with measured results. Though the thickness is not a primary source in propeller loading analysis, experience with propfan acoustics indicates that thickness and lift sources are about equally important.[14]

A three-dimensional time-domain Green's function paneling method[19] similar to that of Morino's[20] has been successfully used to predict the loading and performance for single and counter-rotating propellers. In that calculation, the freestream is parallel to the rotating axis and the loads were assumed identical for all of the blades in the same blade row. Only one blade in each row is used in constructing the influence coefficient matrix. This is not valid when the loads are not blade to blade in phase, e.g., operating in a gust or yawed flow. The influence coefficient matrix must then be constructed by all of the elements on the blades and their wakes. The calculation of the inverse of the influence matrix is inevitably awkward and time consuming, especially when the number of blades is large. In the present study, a three-dimensional frequency-domain method is developed. The axis of rotation is inclined to the freestream, Fig. 1, such that the velocity component of the inflow in the plane of rotation is nonzero. This produces a one cycle per revolution excitation to the blades. The blades are assumed to be identical and rigid, and no aeroelastic effect is included. The main objective of this paper is to describe the computational method in a frequency domain for this problem and present some results obtained from propfan blade SR2 at takeoff and landing speed to quantify the unsteady effect.

Theory and Formulation

In an incompressible, irrotational, and inviscid flowfield, the velocity potential at any instant in time, and any field point, can be expressed in terms of a distribution of sources and doublets over the boundary surface S, which includes all of the blades and their wakes

$$4\pi E\phi(\boldsymbol{x},t) = -\iint \frac{\partial\phi}{\partial n}\frac{1}{R}\,dA + \iint \phi\frac{\partial}{\partial n}\left(\frac{1}{R}\right)dA \qquad (1)$$

where R is the distance between any two points in space and E equals 0 if the field point is inside S, equals ½ if the field point is on S, and equals 1 if it is outside S. The first term on the right side of Eq. (1) represents the source distribution, which is known from the flow tangency boundary condition on the solid surfaces. The second term on the right side represents the unknown doublet distribution. Since we are only interested in the potential distribution on the blade surface, the value of ½ is selected for E in Eq. (1).

The blades are assumed to be identical and rigid. For simplicity, the effects of hub and nacelle are ignored. This assumption should be generally valid unless the shaft angle is sufficiently large that the vorticity generated by the hub and nacelle become important. The wakes of blades are convected downstream, without contraction, by the local freestream.

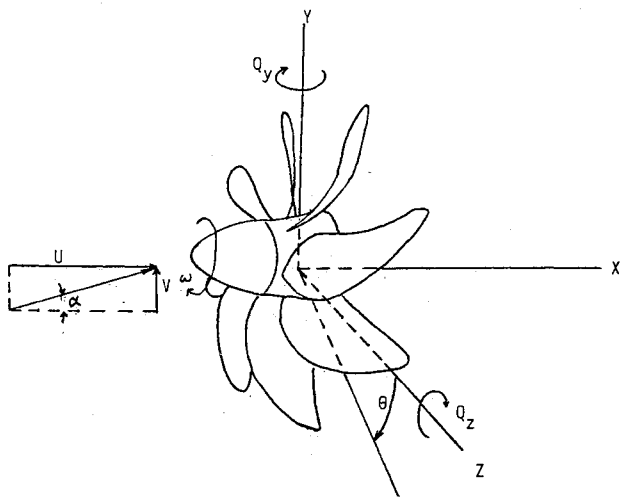

Fig. 1 Inertial coordinate system of rotating blades.

Hence, if there are NB blades, we have NB helical wake surfaces, which are also assumed to be rigid. When the flow is not parallel to the axis, the wakes become skewed helical surfaces. The skewness of the wakes depends on the inclination angle of the rotating axis to the inflow.

Because of the side wind effect, each blade encounters a one cycle per revolution excitation. The blade loadings on the blades are not identical at any instant in time, and there is a phase lag between them. The phase lag between blades can be modeled easily by using an interblade phase angle. The interblade phase angle σ between neighboring blades can be expressed as

$$\sigma = 2\pi/NB \qquad (2)$$

One blade can be picked as the reference blade. The loading on all of the other blades can be expressed in terms of the reference blade with the phase angle at any instant in time.

The boundary condition on the blade surface is the standard flow tangency condition. This yields the blade normal velocity

$$v_n = -\boldsymbol{n}\cdot(\boldsymbol{U}_\infty + \boldsymbol{\omega}\times\boldsymbol{r}) \qquad (3)$$

where $\boldsymbol{n}$ is the blade surface unit normal, $\boldsymbol{U}_\infty$ is the freestream velocity, and $\boldsymbol{r}$ is the blade coordinate vector. Knowing the geometry and motion, Eq. (3) can be written as

$$v_n = -U_x n_x - U_y n_{yz} e^{i(\sigma-\omega t-\pi/2)} - \omega(n_y z - n_z y) \qquad (4)$$

where n_{yz} is the component of $\boldsymbol{n}$ in the YZ plane. The normal velocity includes a time independent (steady) part $v_{n_{st}}$ and a time dependent (unsteady) part $v_{n_{un}}$,

$$v_{n_{st}} = -U_x n_x - \omega(n_y z - n_z y) \qquad (5)$$

$$v_{n_{un}} = -U_y n_{yz} e^{i(\sigma-\omega t-\pi/2)} \qquad (6)$$

Once the interblade phase angle is determined, the unsteady normal velocity on the other blades can be expressed in terms of the reference blade as

$$v_{n_{un}} = v_{n_{un_o}} e^{-i(l-1)\sigma} \qquad (7)$$

The surface of blades and their wakes are subdivided into panels with constant doublet and source strengths. The wake doublet strength near the trailing edge is determined from the numerical Kutta condition, which is represented approximately by

$$\Delta\bar{\phi}_w = \Delta\bar{\phi}_{te} = \bar{\phi}_{te_u} - \bar{\phi}_{te_l} \qquad (8)$$

for steady-state conditions, and by

$$\Delta\tilde{\phi}_w = (\tilde{\phi}_{w_u} - \tilde{\phi}_{w_l}) = (1 - i\omega\Delta t)(\Delta\tilde{\phi}_{te}) \tag{9}$$

for unsteady conditions.

Since the wake doublet strength is determined by the doublet on the blade trailing edge, the phase angle between neighboring blade wakes is also σ. Also, the wake doublet strength is varying periodically with a frequency equal to the upstream disturbance (Fig. 2). There exists a phase lag $\Delta\varphi$ between neighboring wake elements. The phase $\Delta\varphi$ is decided by the disturbing wave length and the time step used to describe the wake sheets, i.e.,

$$\Delta\varphi = 2\pi\Delta t/T \tag{10}$$

Based on the previous assumptions, we can express the entire unsteady wake doublet strength in terms of the doublet strength at the blade trailing edge on the reference blade. Thus, Eq. (1) can be written as

$$[\delta_{ij} - \bar{C}_{ij}]\{\bar{\phi}_j\} - [\bar{W}_{iw}]\{\Delta\bar{\phi}_w\} + [\delta_{ij} - \tilde{c}_{ij}]\{\tilde{\phi}_j\} - [\tilde{w}_{iw}]\{\Delta\tilde{\phi}_w\} = [\bar{B}_{ij}]\{\bar{v}_n\} + [\tilde{b}_{ij}]\{\tilde{v}_n\} \tag{11}$$

where δ_{ij} is the Kronecker Delta function and

$$\bar{C}_{ij} = \frac{1}{2\pi}\sum_l \iint \frac{\partial}{\partial n}\left(\frac{1}{R}\right) dA$$

$$\tilde{c}_{ij} = \frac{e^{i\omega t}}{2\pi}\sum_l \left[e^{-i(l-1)\sigma}\right] \iint \frac{\partial}{\partial n}\left(\frac{1}{R}\right) dA$$

$$\bar{W}_{iw} = \frac{1}{2\pi}\sum_l \sum_{MT} \iint \frac{\partial}{\partial n_w}\left(\frac{1}{R}\right) dA_w$$

$$\tilde{w}_{iw} = \frac{e^{i\omega t}}{2\pi}\sum_l \sum_{MT} \left[e^{-i(l-1)\sigma} e^{-i(NT-MT)\Delta\varphi}\right] \iint \frac{\partial}{\partial n_w}\left(\frac{1}{R}\right) dA_w$$

$$\bar{B}_{ij} = -\frac{1}{2\pi}\sum_l \iint \left(\frac{1}{R}\right) dA$$

$$\tilde{b}_{ij} = \frac{-e^{i\omega t}}{2\pi}\sum_l e^{-i(l-1)\sigma} \iint \left(\frac{1}{R}\right) dA$$

The unsteady loads induced by the yawed flow can be decoupled mathematically from the steady loads, that is,

$$[\delta_{ij} - \bar{C}_{ij}]\{\bar{\phi}_j\} - [\bar{W}_{iw}]\{\Delta\bar{\phi}_w\} = [\bar{B}_{ij}]\{\bar{v}_n\} \tag{12}$$

$$[\delta_{ij} - \tilde{c}_{ij}]\{\tilde{\phi}_j\} - [\tilde{w}_{iw}]\{\Delta\tilde{\phi}_w\} = [\tilde{b}_{ij}]\{\tilde{v}_n\} \tag{13}$$

For the steady part, Eq. (12) gives the steady solution $\bar{\phi}_j$ and Eq. (13) gives the unsteady solution $\tilde{\phi}_j$. The overall velocity potential is simply the superposition of steady and unsteady solutions, i.e.,

$$\phi_j = \bar{\phi}_j + \tilde{\phi}_j e^{i\omega t} \tag{14}$$

The pressure is calculated using the unsteady Bernoulli's equation once the velocity potential is obtained,

$$\frac{p'}{\rho} = \frac{p - p_\infty}{\rho} = -\frac{\partial\phi}{\partial t} - U_\infty \cdot \nabla\phi - \frac{1}{2}|\nabla\phi|^2 \tag{15}$$

The pressure coefficient is nondimensionized by the axial inflow dynamic pressure

$$C_p = p'/\tfrac{1}{2}\rho U_x^2 \tag{16}$$

The thrust and power can be calculated by summing the forces in the axial and tangential directions. The thrust and power coefficients for the rotor are

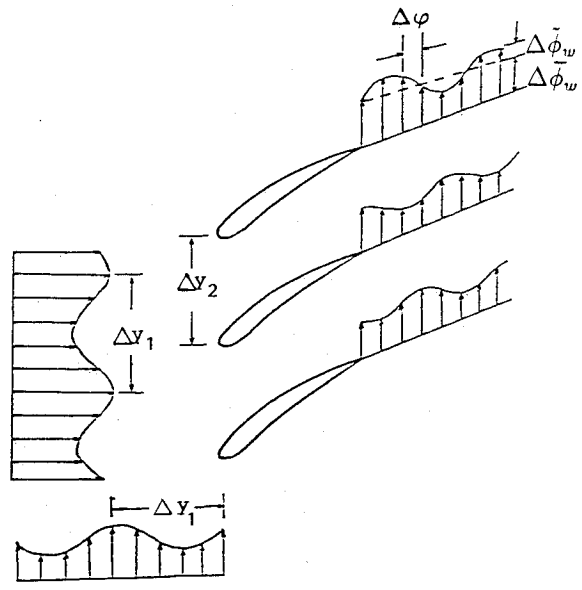

Fig. 2 Gust and unsteady wake model.

$$C_T = \frac{T}{\rho\Omega^2 D^4} = \frac{\sum_{NB}\sum_i \left[C_p n_x \Delta A)_u + (C_p n_x \Delta A)_l\right]_i U_x^2}{32\Omega^2 r_{tip}^4} \tag{17}$$

$$C_P = \frac{P}{\rho\Omega^3 D^5} = \frac{\sum_{NB}\sum_i \pi\left[C_p \Delta A (n_z y - n_y z)\right]_i U_x^2}{32\Omega^2 r_{tip}^5} \tag{18}$$

The force produced by the yawed flow is asymmetric to the plane of rotation. The torques generated by the nonaxisymmetric force with respect to the Y and Z axes are represented as nondimensional torque coefficients,

$$C_{Q_y} = \frac{Q_y}{\rho\Omega^2 D^5} = \sum_{NB}\sum_{iz} \Delta C_T \cdot \frac{z}{D} \tag{19}$$

$$C_{Q_z} = \frac{Q_z}{\rho\Omega^2 D^5} = \sum_{NB}\sum_{iz} \Delta C_T \cdot \frac{y}{D} \tag{20}$$

where ΔC_T is the differential thrust along the blade span and iz is the blade radial index.

Results and Discussion

Single-rotation propfan blade SR2 was used to test this method. When there is no shaft inclination, $\alpha = 0$, the blade loadings are identical for all of the blades and are independent of time. The predicted steady results are identical for both the time domain (at a converged solution) and the frequency domain. Figure 3 shows the pressure distribution at different spanwise locations of an eight-bladed SR2 at $\beta_{3/4} = 40.3$ deg, advance ratio 1.633. The comparison with the lifting surface theory[18] in the same figure indicates that they are in excellent agreement from hub to tip. The radial distribution of thrust (Fig. 4) shows very good agreement again between the present method and the lifting surface method. Figures 5 and 6 show the overall thrust and power coefficients in comparison to the lifting surface theory. The two methods agree well though the lifting surface predicted lower power at lower advance ratio. In addition, measured values of net power are shown in Fig. 6. Both the present incompressible method and the lifting surface theory underpredict the power at higher loading. This is due both to the inviscid rigid wake model and Mach number effect. The two-dimensional strip fashion Prandtl-Glauert (P-G) compressibility correction technique that was used successfully to predict the propfan performance by Kobayakawa and Onuma[10] is also employed here. Figure 6 shows that the corrected

powers move closer to the measured results, especially at lower advance ratios, with relative Mach number equal to 0.81 at $J=0.8$ and $M=0.2$. Less changes were found for higher advance ratios since the relative Mach numbers are smaller for a given axial Mach number. The two-dimensional compressibility correction method is basically utilized to avoid the difficulties associated with solving directly the three-dimensional compressible flow problems. It is valid for most subsonic flow but failed for transonic or supersonic conditions. For most conditions, yaw flow effect is significant like ascending, descending, etc., the use of P-G transformation should be generally good. The following calculation is based on incompressible flow analysis, but the effect of compressibility in unsteady response will be discussed in the last part of this section.

The unsteady load prediction is first tested on a two-bladed SR2 with a shaft angle of 3 deg. The time-domain calculation is started from rest. The wake of the rotor is generated step by step, convected downstream with freestream velocity and gradually changes into a skewed helical surface. As the transient solution is not the main interest of the present study, the time-marching solution uses a sufficiently small time step, $\Delta t=0.02D/U_x$, to adequately model the helical wake surfaces, but not enough to resolve a good transient solution from the start. In Fig. 7, the unsteady load reaches cyclic condition soon after the blades start rotating. The loading on blade 1 is 180 deg out of phase in comparison to that of blade 2. The time history shows little difference compared with the result from the frequency-domain calculation. The CPU time for a 128-panel blade and 80 wake time steps is about 11 min on an APOLLO-4000 workstation for the present frequency-domain analysis and is about 10 h for the time-domain computation. The difference is even larger for a rotor with more blades since the influence matrix size is proportional to the blade number for the time-domain calculation. Also, the influence domain calculates only once at any arbitrary reference time, whereas the time domain is required to start from rest and stop when a converged solution is obtained. Thus, the advantage for the frequency-domain analysis is obvious.

The differential thrust on the reference blade with a 3-deg shaft angle (on an eight-bladed rotor) at different circumferential locations is shown in Fig. 8. This shows a strong one cycle

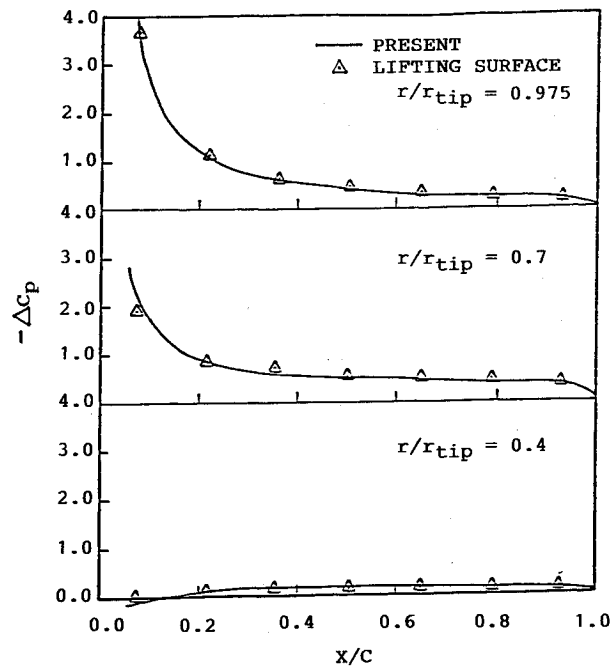

Fig. 3 Pressure distribution on single rotation SR2: $\beta_{3/4}=40.3$ deg; $NB=8$; $J=1.633$.

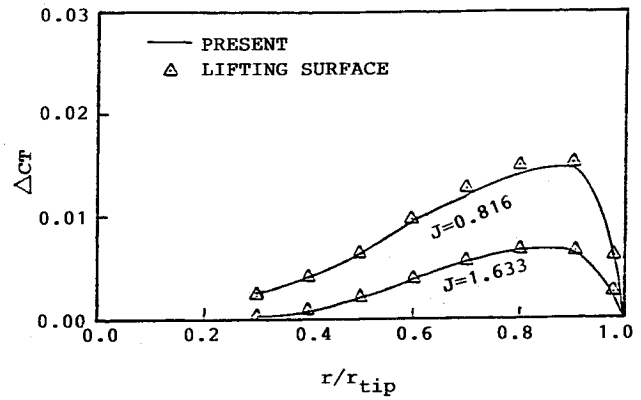

Fig. 4 Differential thrust on SR2.

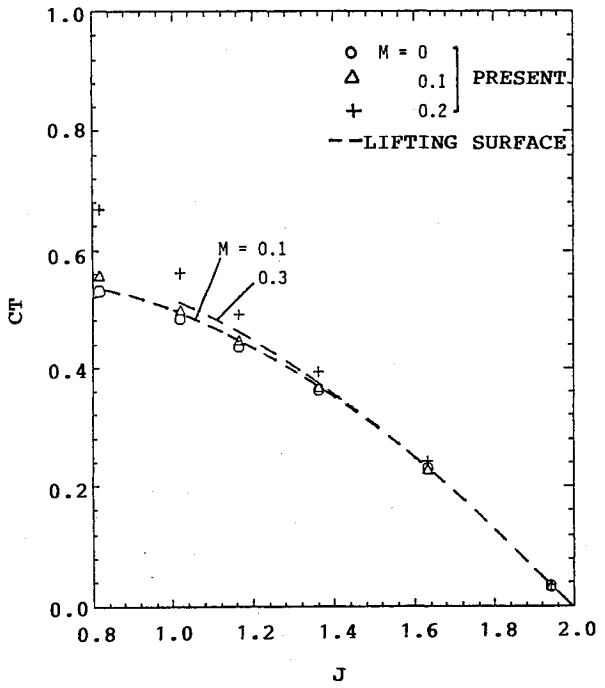

Fig. 5 Comparison of predicted thrust.

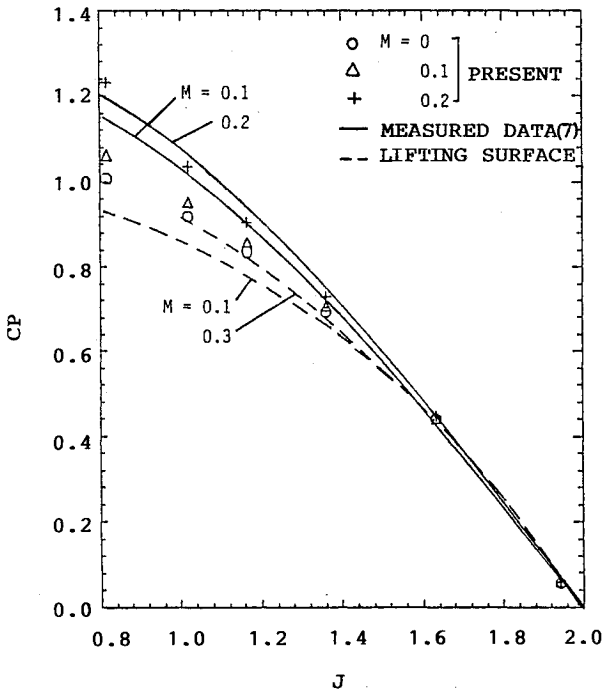

Fig. 6 Comparison of predicted and measured power.

per revolution behavior with the blade maximum load occurring around 0 deg with the largest local angle of attack, and the minimum load occurring around 180 deg with minimum local angle of attack. Negative differential thrust shown in the figure is mainly due to locally negative incidence.

As the force produced by the side wind effect is dependent on blade azimuth location and is asymmetric to any of the three axes, the torque produced by the blades are nonzero. Figure 9 shows the torques with respect to the Y and Z axes, Q_y and Q_z, increase with the blade number while the thrust-to-blade ratio decreases as number of blades increase. The overall forces and torques are more or less constant in time (within 1% of variation) except when $NB = 2$. This is because the blades are equally spaced and the unsteady loading is nearly sinusoidal. Figure 10 shows that, by increasing the number of blades on a rotor, the blade mean loading decreases but the unsteady loading increases. Relatively, the change in mean

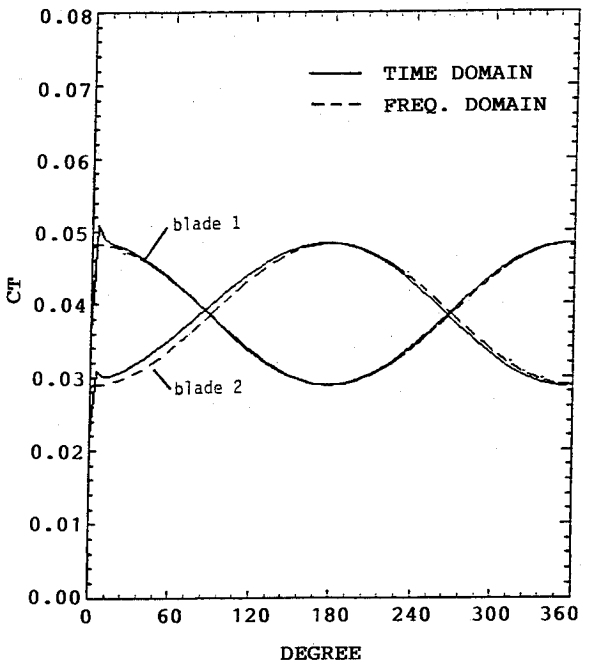

Fig. 7 Time-domain vs frequency-domain thrust calculation for one revolution: $J = 1.633$.

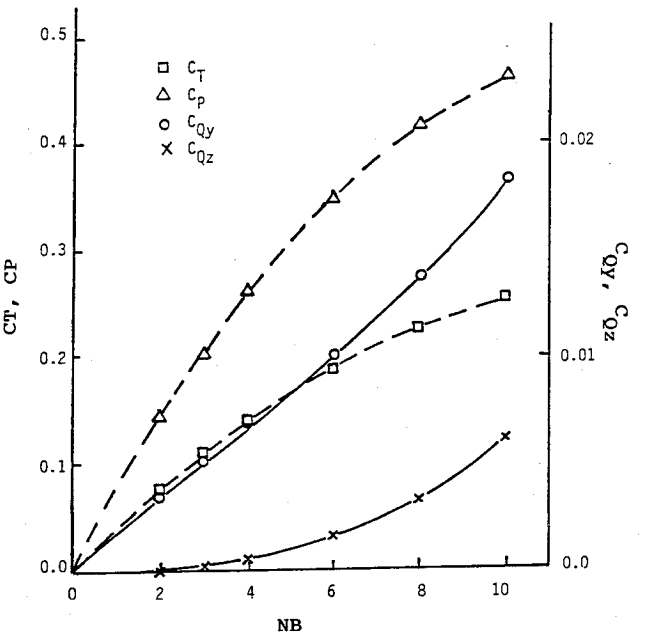

Fig. 9 Forces and torques produced by off-axis inflow.

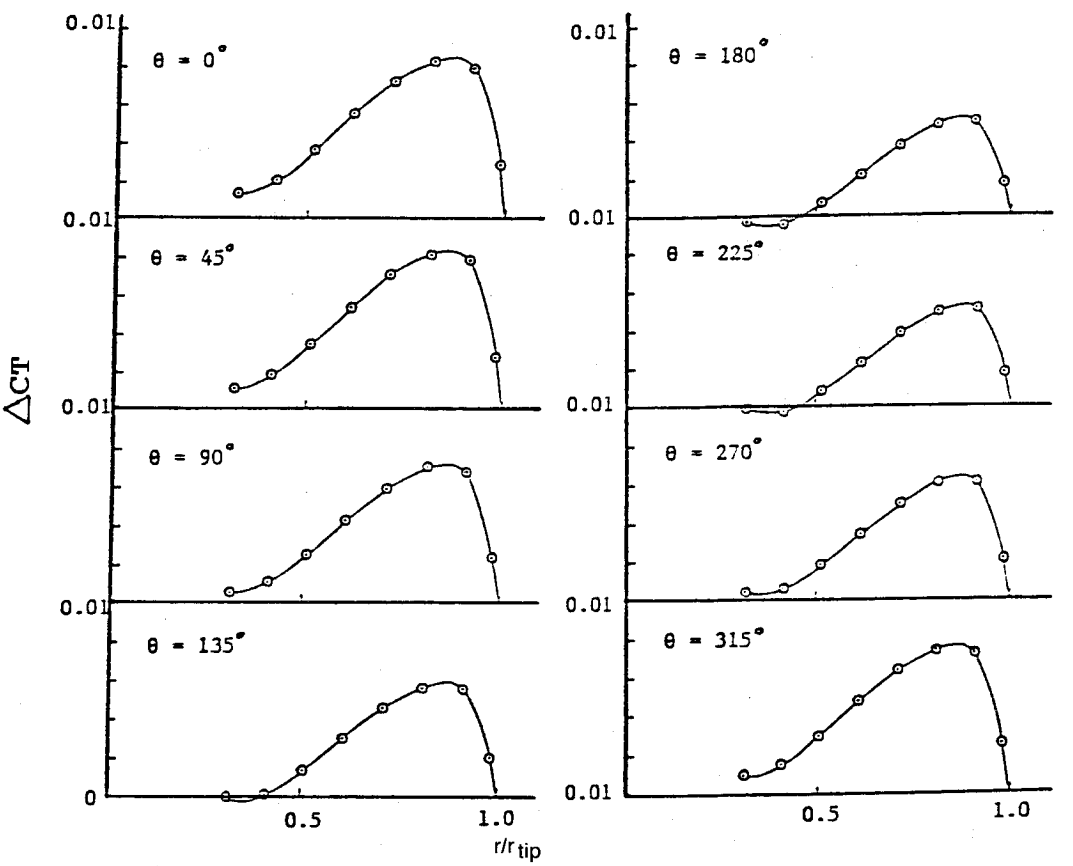

Fig. 8 Differential thrust on reference blade at different circumferential locations: $J = 1.633$.

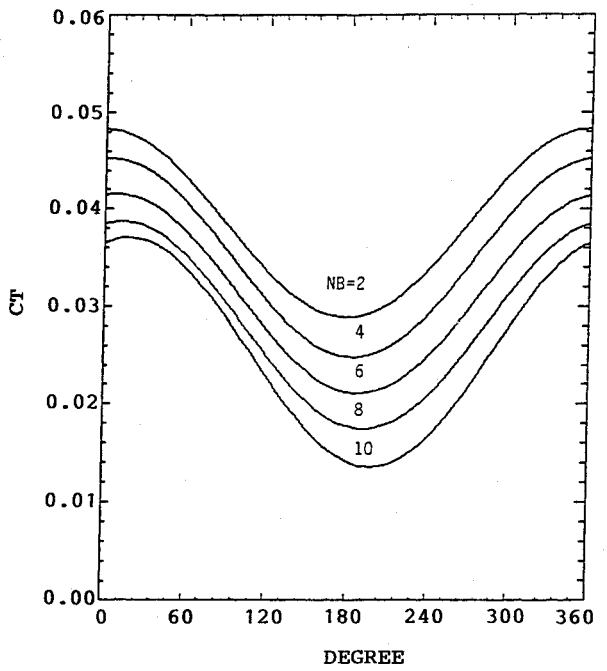

Fig. 10 Number of blade effect on unsteady loading.

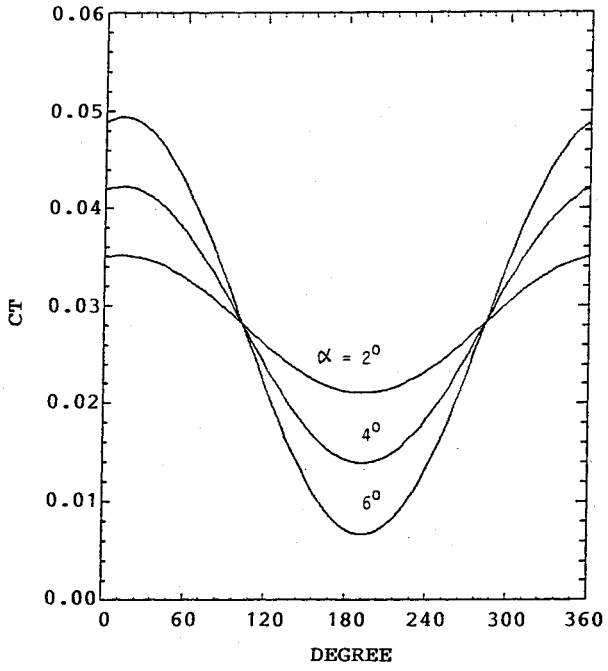

Fig. 11 Shaft angle-of-attack effect on unsteady loading.

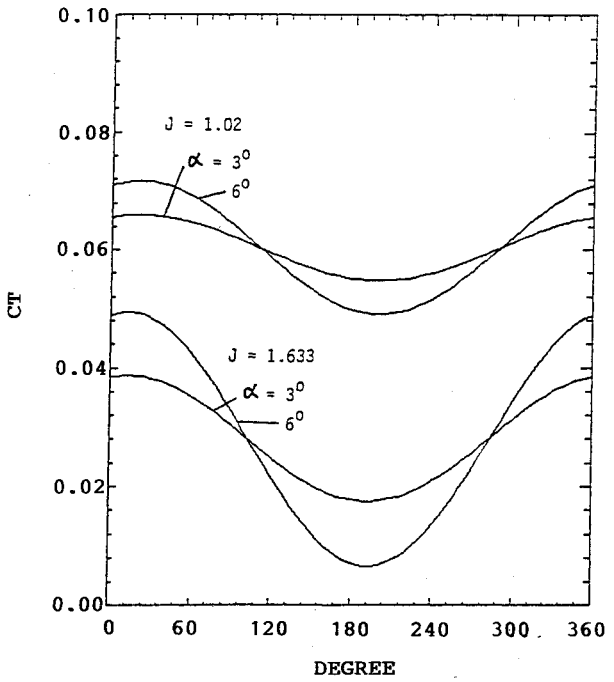

Fig. 12 Advance ratio effect on unsteady loading.

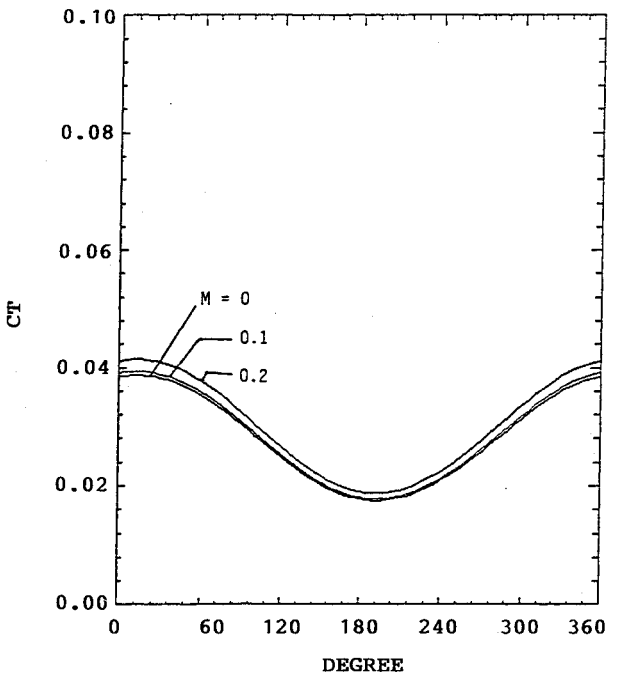

Fig. 13 Mach number effect on unsteady loading: $J = 1.633$; $\alpha = 3$ deg.

loading is more significant than that of the unsteady part by changing the blade number. The curves of unsteady loading shift due to the interaction between blades becomes stronger as the blade number increases.

The unsteady loadings for one cycle of revolution at different shaft angles, 2, 4, and 6 deg, are shown in Fig. 11. The peak-to-peak amplitude is comparable to the mean loading at that operating condition. This indicated that the unsteady loading is sensitive to the shaft angle and the magnitude of excess unsteady load on a single blade is proportional to the degree of axis inclination (with nonlinearity only 1.1% at 6 deg by using skewed helical wake); this agreed with the observation by Mehmed et al.[3]

Figure 12 shows that the unsteady load variation at the same shaft angle is lower for a smaller advance ratio. This is due to a smaller ratio of the in-plane transverse velocity to rotational speed. The effective cyclic flow angle-of-attack change is smaller and, thus, the lower unsteady load variation results.

The compressibility effect for the yawed flow is corrected in the same way as that used in the steady analysis. Figures 13–15 show the correction at axial Mach number 0.1 and 0.2 at two advance ratios ($J = 1.02$ and 1.633) and two shaft angles ($\alpha = 3$ and 6 deg). In these figures, the unsteady loads are more significant at $\theta = 0$ because the relative Mach number at this blade azimuth position is higher than that when $\theta = 180$ deg. For the higher advance ratio $J = 1.633$, the unsteady load is dominated more by the shaft angle of attack than by the Mach number as seen from Figs. 13 and 14. Similarly, Fig. 15 shows, for the lower advance ratio, $J = 1.02$, that the unsteady load variation due to the Mach number effect is similar to that of a higher advance ratio, though the mean loading is signifi-

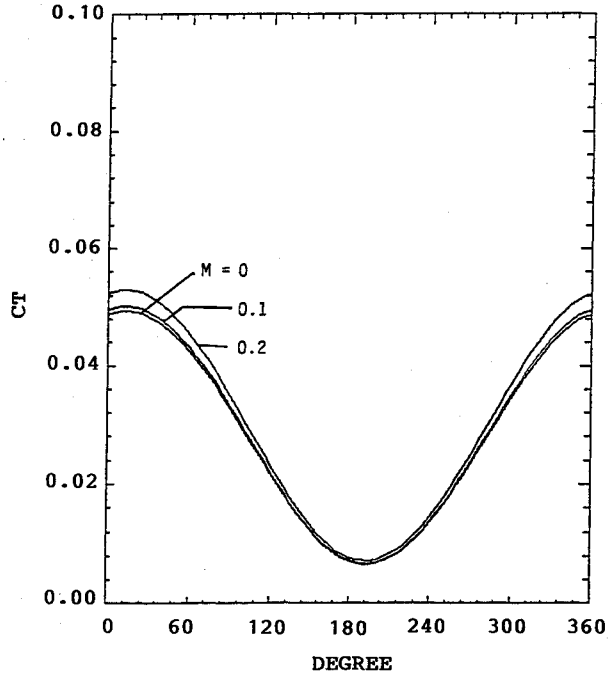

Fig. 14 Mach number effect on unsteady loading: $J = 1.633$; $\alpha = 6$ deg.

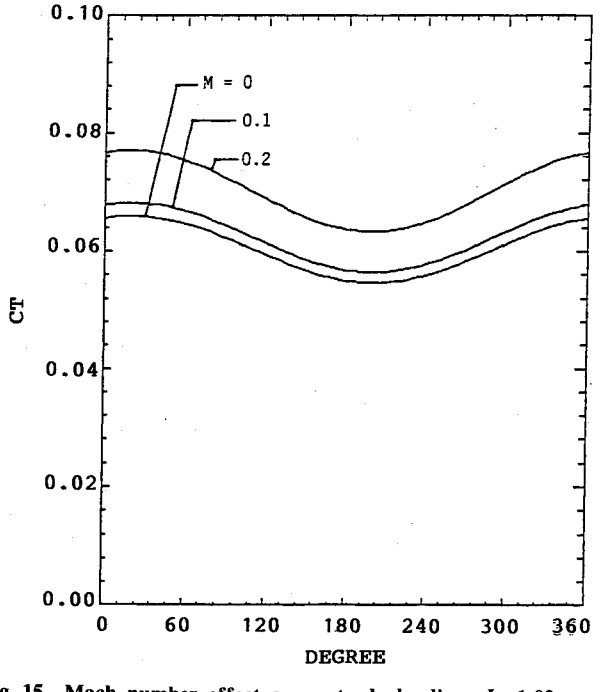

Fig. 15 Mach number effect on unsteady loading: $J = 1.02$; $\alpha = 3$ deg.

cantly higher. Thus, the effect of Mach number on unsteady loading is less significant than that of shaft angle of attack change.

Conclusions

The results presented here indicate that the frequency-domain source and doublet potential paneling method can be used to predict the propfan one cycle per revolution unsteady loading with axis of rotation not parallel to the inflow. The comparison with the results from a time-domain calculation is good and its computation is very efficient.

The analysis is based on incompressible flow theory though compressibility is corrected in a two-dimensional fashion to account for the fact that the propfan is designed to fly at high subsonic speeds. The unsteady loading based on the calculation for a single rotation SR2 propfan is found to be dependent on the angle between inflow and axis of blade rotation, advance ratio, number of blades, and axial Mach number. Among them, the shaft angle seems to be the dominant parameter in the yawed flow problem. Relatively, the Mach number effect is the least influential. Since little data is available on the off-axis flow problem, measurements are needed to properly assess the validity of the method and provide a baseline for compressibility corrections.

References

[1]Saito, S., Kobayashi, H., Nakamura, Y., and Matsuo, Y., "Predicted Flow Field Around the Advanced Propeller at Take-off," AIAA Paper 88-3151, July 1988.

[2]August, R., and Kaza, K. R. V., "Vibration, Flutter Performance and Forced Response Characteristics of a Large Scale Propfan and Its Aeroelastic Model," AIAA Paper 88-3155, July 1988.

[3]Mehmed, O., "Experimental Investigation of Propfan Aeroelastic Response in Off-Axis Flow with Mistuning," AIAA Paper 88-3153, July 1988.

[4]Kaza, K. R. V., Williams, M. H., Mehmed, O., and Marayanan, G., "Aeroelastic Response of Metallic and Composite Profan Models in Yawed Flow," AIAA Paper 88-3154, July 1988.

[5]Padula, S. L., and Block, P. J. W., "Predicted Changes in Advanced Turboprop Noise with Shaft Angle of Attack," AIAA Paper 84-2347, Oct. 1984.

[6]Block, P. J. W., "Noise Radiation Patterns of Counter-Rotation and Unsteadily Loaded Single-Rotation Propellers," *Journal of Aircraft,* Vol. 22, No. 9, 1985, pp. 776–783.

[7]Stefko, G. L., and Jeracki, R. J., "Wind-Tunnel Results of Advanced High-Speed Propellers at Takeoff, Climb, and Landing Mach Numbers," NASA TM-87030, Nov. 1985.

[8]Metzger, F. B., and Brown, P. C., "Results of Acoustic Tests of a Prop-Fan Model," *Journal of Aircraft,* Vol. 25, No. 7, 1988, pp. 653–658.

[9]Nallasamy, M., Woodward, R. P., and Groeneweg, J. F., "High Speed Propeller Performance and Noise Predictions at Takeoff-Landing Conditions," *Journal of Aircraft,* Vol. 26, No. 6, 1989, pp. 563–569.

[10]Kobayakawa, M., and Onuma, H., "Propeller Aerodynamic Performance by Vortex Lattice Method," *Journal of Aircraft,* Vol. 22, No. 8, 1985, pp. 649–654.

[11]Jou, W. H., "Finite Volume Calculation of 3-D Potential Flow Around a Propeller," *AIAA Journal,* Vol. 21, No. 10, 1983, pp. 1360–1365.

[12]Chang, L. K., "The Theoretical Performance of High Efficiency Propellers," Ph.D. Dissertation, School of Aeronautics and Astronautics, Purdue University, West Lafayette, IN, 1980.

[13]Bober, L. J., Chaussee, D. S., and Kutler, P., "Prediction of High Speed Propeller Flow Fields Using a Three-Dimensional Euler Analysis," NASA TM-83065, Jan. 1983.

[14]Hanson, D. B., "Compressible Helicoidal Surface Theory for Propeller Aerodynamics and Noise," *AIAA Journal,* Vol. 21, No. 6, 1983, pp. 881–889.

[15]Lesieutre, D. J., and Sullivan, J. P., "Unsteady Forces on Counter Rotating Propeller Blades," AIAA Paper 86-1804, June 1986.

[16]Celestina, M. L., Mulac, R. A., and Adamczyk, J. J., "A Numerical Simulation of the Inviscid Flow Through a Counter-Rotating Propeller," *Journal of Turbomachinery, Transactions of the ASME,* Vol. 108, No. 4, 1986, pp. 187–193.

[17]Whitfield, D. L., Swafford, T. W., Janus, J. M., Mulac, R. A., and Belk, D. M., "Three-Dimensional Unsteady Euler Solution for Propfans and Counter-Rotating Propfans in Transonic Flow," AIAA Paper 87-1197, June 1987.

[18]Williams, M. H., and Hwang, C. C., "Three-Dimensional Unsteady Aerodynamic and Aerolastic Response of Advanced Turboprops," AIAA Paper 86-0846, May 1986.

[19]Chen, S. H., and Williams, M. H., "A Panel Method for Counter Rotating Profans," AIAA Paper 87-1890, June 1987.

[20]Morino, L., "A General Theory of Unsteady Compressible Potential Aerodynamics," NASA CR-2464, Dec. 1974.